Joint inversion of velocity and density in preserved-amplitude full waveform inversion

Botao Qin, Gilles Lambaré, CGG*

Summary

The importance of joint inversion for velocity and density in full waveform inversion (FWI) is well established. In an earlier work we proposed a preserved-amplitude FWI allowing an improved convergence rate for FWI. This was derived from preserved-amplitude reverse time migration (RTM) using a deconvolution imaging condition, and it was limited to the estimation of velocity perturbation from reflection data. Here we extend the approach to a joint velocity and density preserved-amplitude FWI. We derive expressions for the improved common-shot FWI gradients, and show how we can decouple the two parameters. We validate our approach on (1) a synthetic model, showing that we can efficiently reconstruct the two parameters, and (2) a field dataset, showing that we significantly reduce the data residual with the joint inversion.

Introduction

The benefit of introducing a density or a pseudo-density term in FWI has been frequently highlighted (Przebindowska et al., 2012; Plessix et al., 2013; Guitton, 2014). While velocity affects traveltimes and amplitudes along the wave trajectories, density contrasts mainly affect the amplitudes of reflected waves. Therefore, ignoring the effects of density on reflection amplitudes creates the potential for density leakage into the velocity update (Kumar et al., 2014). However, it is difficult to correctly reconstruct density in FWI since its effects on reflected waves are coupled with those of velocity (Forgues and Lambaré, 1997; Virieux and Operto, 2009), producing crosstalk in the inversion. Several approaches have been proposed, such as Jeong and Min (2012) with a hierarchical strategy or Bai and Yingst (2014) with a simultaneous inversion using preconditioned velocity and density gradients. None of these approaches is able to efficiently solve the crosstalk problem; only through a large number of iterations in the optimization process can the crosstalk between parameters be reduced.

Qin et al. (2015) proposed a preserved-amplitude FWI, providing improved expressions for the velocity component of the FWI gradient. Our approach, which was based on a high-frequency asymptotic formulation, significantly improves the convergence rate of FWI for reflected waves. In this abstract, we extend our method to joint velocity and density inversion. This is similar to the proposal of Zhang et al. (2014) for angle-domain RTM-based FWI, which estimated impedance and velocity perturbations. Our approach is based on common-shot migration using a deconvolution imaging condition, and it offers the advantages of efficiency and robustness.

We begin by recalling preserved-amplitude FWI. Then we derive the inversion formula to estimate velocity and density perturbations based on the Born approximation, and show how to incorporate them into the preserved-amplitude FWI workflow. Finally, we show results obtained on the Marmousi II dataset and a 2D marine field dataset.

Theory

The acoustic wave equation governing the propagation of seismic waves in an isotropic medium reads

$$\left(\frac{1}{K(\boldsymbol{x})}\frac{\partial^2}{\partial t^2}-\nabla\frac{1}{\rho(\boldsymbol{x})}\cdot\nabla\right)p(\boldsymbol{x};t;\boldsymbol{s})=\delta(\boldsymbol{x}-\boldsymbol{s})\delta(t), \quad (1)$$

where $\boldsymbol{s}$ is the shot position, $K(\boldsymbol{x})$ and $\rho(\boldsymbol{x})$ denote the bulk modulus and the density, respectively. Velocity is connected to bulk modulus and density through $v^2(\boldsymbol{x})=K(\boldsymbol{x})/\rho(\boldsymbol{x})$.

For reference bulk modulus and density models (K_0,ρ_0), $(\delta K,\delta\rho)=(K-K_0,\ \rho-\rho_0)$ denotes the model perturbations. We consider the first-order Born approximation. The perturbation of the acoustic wavefield emitted at a source point $\boldsymbol{s}$ and recorded at a receiver position $\boldsymbol{r}$, $\delta p(\boldsymbol{r},\omega;\boldsymbol{s})$, satisfies (Tarantola, 1984):

$$\delta p(\boldsymbol{r};\omega;\boldsymbol{s})=-\omega^2\iiint d\mathbf{x}\quad G_0(\boldsymbol{x};\omega;\boldsymbol{s})\quad G_0(\boldsymbol{x};\omega;\boldsymbol{r})\frac{\delta K(\boldsymbol{x})}{K_0^2(\boldsymbol{x})} \quad (2)$$
$$+\quad\iiint d\mathbf{x}\ \ \nabla G_0(\boldsymbol{x};\omega;\boldsymbol{s})\cdot\nabla G_0(\boldsymbol{x};\omega;\boldsymbol{r})\frac{\delta\rho(\boldsymbol{x})}{\rho_0^2(\boldsymbol{x})}$$

where G_0 denotes the Green function in the reference models. Introducing a high-frequency approximation, we obtain (Forgues and Lambaré, 1997)

$$\delta p(\boldsymbol{r};\omega;\boldsymbol{s})=-\omega^2\iiint d\mathbf{x}\left(\frac{\delta K(\boldsymbol{x})}{K_0(\boldsymbol{x})}+\cos\left(\Theta(\boldsymbol{s},\boldsymbol{x},\boldsymbol{r})\right)\frac{\delta\rho(\boldsymbol{x})}{\rho_0(\boldsymbol{x})}\right) \quad (3)$$
$$\frac{G_0(\boldsymbol{x};\omega;\boldsymbol{s})G_0(\boldsymbol{x};\omega;\boldsymbol{r})}{K_0(\boldsymbol{x})}$$

where $\Theta(\boldsymbol{s},\boldsymbol{x},\boldsymbol{r})$ denotes angle at point $\boldsymbol{x}$ between incident ray from the source and the reflected ray to the receiver. We assume that for each shot, at any position $\boldsymbol{x}$ a single specular aperture angle exists. Such assumption is reasonable in most cases. Then we can define the angle-dependent diffracting kernel, $M(\boldsymbol{x},\boldsymbol{s})$, as

$$M(\boldsymbol{x},\boldsymbol{s})=\frac{\delta K(\boldsymbol{x})}{K_0(\boldsymbol{x})}+\cos\left(\Theta(\boldsymbol{s},\boldsymbol{x},\boldsymbol{r})\right)\frac{\delta\rho(\boldsymbol{x})}{\rho_0(\boldsymbol{x})}. \quad (4)$$

Qin et al. (2015) (based on Beylkin, 1985 and Bleistein et al., 2001) provided an approximation for $M(\boldsymbol{x},\boldsymbol{s})$ through the common-shot preserved-amplitude FWI formula. Within high-frequency asymptotic theory we have

$$M(\boldsymbol{x},\boldsymbol{s})\approx\frac{iK_0}{2\pi\rho_0}\int d\omega\ \frac{\nabla p_B\cdot\nabla\overline{p}_F+p_B\nabla^2\overline{p}_F}{\omega^3 p_F\overline{p}_F}, \quad (5)$$

where p_F denotes the forward propagated source wavefield and p_B denotes the backward propagated residual wavefield.

Assuming we have a way to compute cosΘ, we have now all the tools to build an inversion algorithm for the δK and $\delta\rho$ perturbations. We are looking for $\delta K/K_0$ and $\delta\rho/\rho_0$ from a set of $M_i=M(\boldsymbol{x},\boldsymbol{s}_i)$ and $c_i=\cos\Theta(\boldsymbol{s}_i)$ recovered from a set of shots, $\boldsymbol{s}_i$, $i=1, N_s$. This can be considered as a linear inverse problem whose solution can be expressed explicitly for any position in the image as

$$\begin{pmatrix} \delta K/K_0 \\ \delta\rho/\rho_0 \end{pmatrix} = \left(\sum_{i=1}^{N_s} W_i \begin{pmatrix} 1 & c_i \\ c_i & c_i^2 \end{pmatrix} \right)^{-1} \sum_{i=1}^{N_s} \left(\begin{pmatrix} 1 \\ c_i \end{pmatrix} W_i M_i \right). \quad (6)$$

where $W_i=W(\boldsymbol{x},\boldsymbol{s}_i)$ is a (preconditioning) weight function. Note that bulk modulus and density perturbation can be converted to any other pair of parameters, e.g., impedance-density, impedance-velocity, or slowness-density.

There are several ways of estimating cosΘ. One possibility is the migration of attribute proposed by Bleistein (1987) and used for aperture angle map computation for AVO or surface offset domain RTM (Giboli et al., 2012). Indeed, within the high-frequency asymptotic approximation the ratio between two components summed in the right side of formula (5) provides this angle information. Another possibility is the approach proposed by Guitton (2004). The obtained gradient is used alternatively as velocity and density perturbations to simulate data and then the ratio of the two new images provides cosΘ. In the examples in this paper, we use common-shot tomographic ray tracing to produce the angle map (based on a dip model). Both the approximation errors in angle estimation and the effects of the degradation of the validity of the single-specular-angle assumption will be corrected by the iterative process.

Examples

To demonstrate the reliability of our method compared with single parameter inversion, we first apply it to the synthetic Marmousi II model (Martin et al., 2006). The exact velocity and density models were extended laterally and a 500 m thick water layer was added on top. The data were generated by finite difference modeling for a towed marine streamer acquisition with offsets ranging from 0 to 3 km. The source function was a Dirac function band-pass filtered within [3, 30] Hz. High-definition tomography (Guillaume et al., 2012) was applied to obtain the initial velocity model, Figure 1(a). The initial density model was obtained by heavy smoothing of the exact density model. We performed a 20 Hz velocity-only preserved-amplitude FWI with a fixed smooth density model, and a velocity and density joint update inversion. Figures 1(c) and 1(d) show the recovered velocity perturbation after iterations. We see that the velocity perturbation obtained by joint inversion is generally higher than the velocity perturbation obtained by the velocity-only inversion. It is also closer to the true perturbation, Figure 1(b). This is confirmed by comparison at wells shown in Figure 3. The joint update also produces a reliable density perturbation, Figure 2(a). The large density contrasts are recovered compared to exact perturbation in Figure 2(b), and comparisons at wells show reasonable matches. The cost function in FWI is significantly reduced with joint inversion, Figure 2(c).

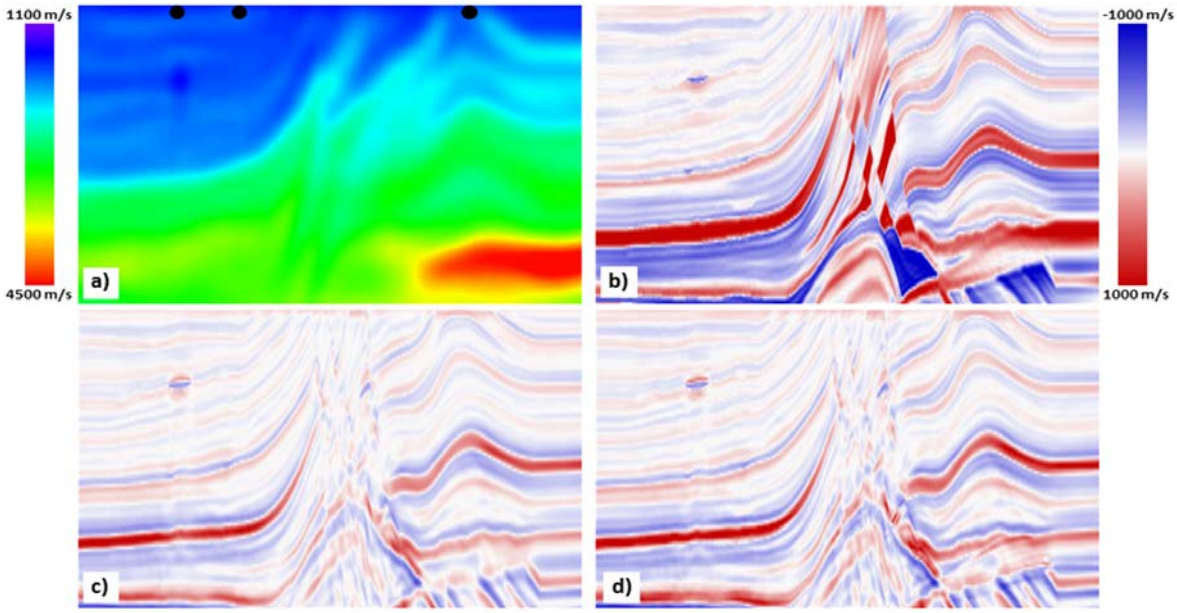

Figure 1: Test on Marmousi II model. (a) Initial velocity built from tomography, the three black dots mark well locations displayed in Figure 3; (b) True velocity perturbation; (c) Velocity perturbation from 20 Hz velocity-only inversion; (d) Velocity perturbation from 20 Hz joint inversion.

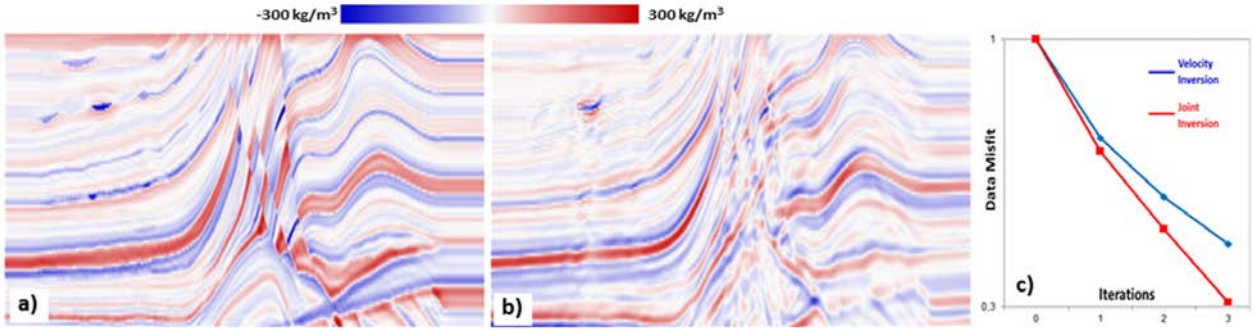

Figure 2: Test on Marmousi II model. (a) True density perturbation; (b) Density perturbation from 20 Hz joint inversion; (c) Cost functions for the two tests: velocity-only inversion (blue) and joint inversion (red).

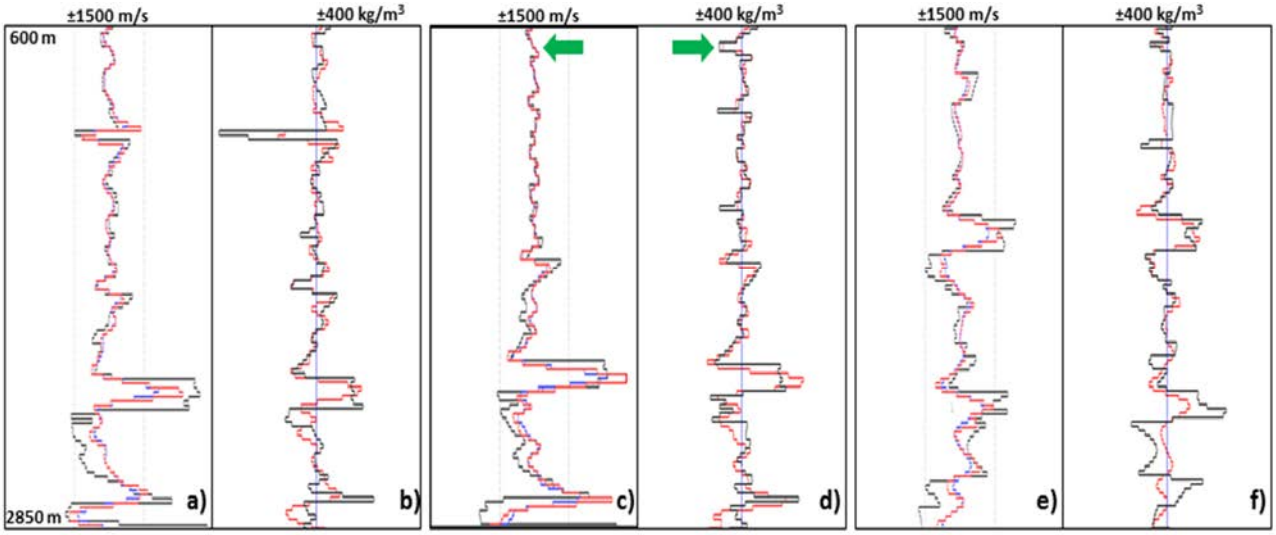

Figure 3: Test on Marmousi II model. Detailed comparisons of true perturbations (black), velocity-only inversion perturbations (blue) and joint inversion perturbations (red). Velocity (a) and density (b) perturbations at well location indicated by the left black dot in Figure 1(a); velocity (c) and density (d) perturbations at well location indicated by the middle black dot in Figure 1(a). The green arrows in (c) and (d) highlight correct recovery of opposite signs of velocity perturbation and density perturbation; velocity (e) and density (f) perturbations at well location indicated by the right black dot in Figure 1(a).

We then applied our approach to a 2D broadband marine field dataset acquired offshore Australia (1240 shots spaced by 37.5 m with a maximum offset of 7 km). The initial velocity model (Figure 4(a)) was obtained by ray-based tomography. An initial density model was derived from Gardner's law (Gardner et al., 1974). We first performed a 20 Hz velocity-only inversion. The density was updated after each iteration, again by Gardner's law. The velocity perturbation is shown in Figure 4(c). Then we performed a 20 Hz joint update inversion. The velocity and density perturbations are shown in Figures 4(b) and 4(d). The improved convergence appears as a bigger and faster decrease of the cost function shown on Figure 5 (left). Figure 5 (right) and Figure 6 show comparisons between modeled data and field data, and highlight the improvement produced by the joint velocity and density inversion.

Conclusions

In seismic data interpretation for oil and gas exploration, density as well as velocity is needed. One challenge for FWI is to recover a reliable density model. We have developed a theory of shot-domain preserved-amplitude FWI to delineate both velocity and density perturbations, reducing the velocity / density crosstalk. Synthetic and field examples have shown that the proposed method is reliable and can provide better convergence than velocity-only FWI.

Acknowledgements

We thank Sam Gray, Francesco Perrone, Chu-Ong Ting for helpful discussions. We thank CGG for the permission to publish this work and for providing the field dataset.

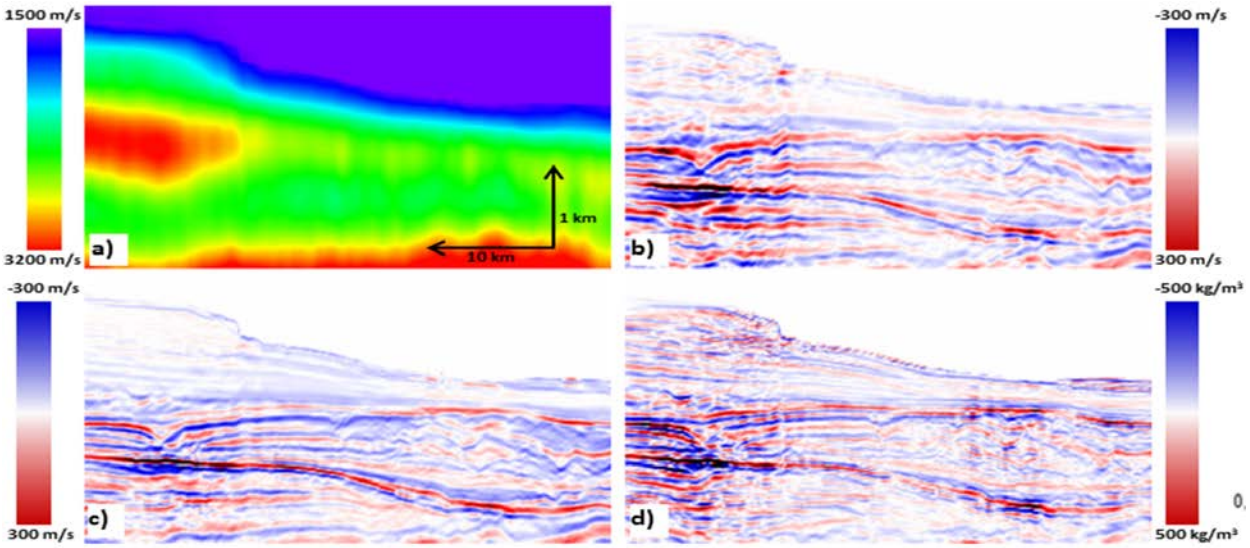

Figure 4: Field dataset application. (a) Initial velocity model from tomography; (b) Velocity perturbation from 20 Hz joint inversion; (c) Velocity perturbation from 20 Hz velocity-only inversion; (d) Density perturbation from 20 Hz joint inversion.

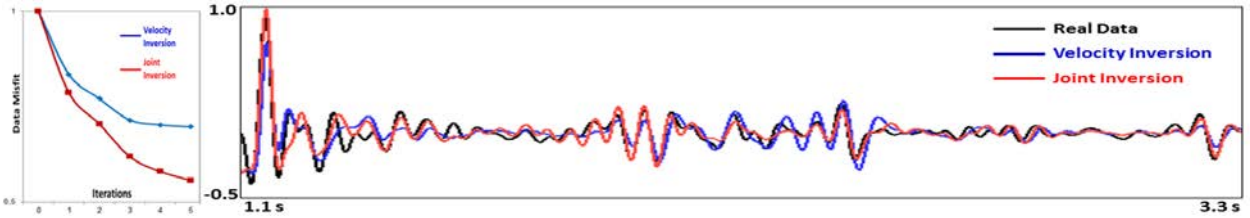

Figure 5: Field dataset application. Left) Cost function for the two tests. Right) A near offset trace comparison between field and modeled data.

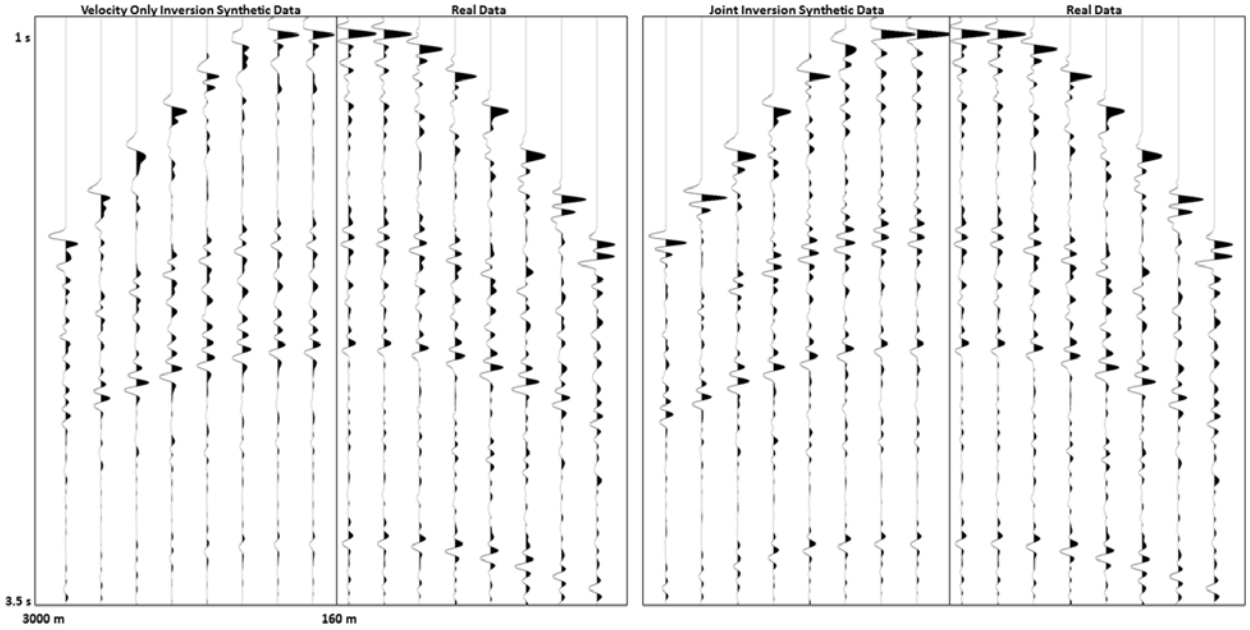

Figure 6: Field dataset application. Modeled data and field data comparisons at offset range [160, 3000] m.

EDITED REFERENCES

Note: This reference list is a copyedited version of the reference list submitted by the author. Reference lists for the 2016 SEG Technical Program Expanded Abstracts have been copyedited so that references provided with the online metadata for each paper will achieve a high degree of linking to cited sources that appear on the Web.

REFERENCES

Bai, J., and D. Yingst, 2014, Simultaneous inversion of velocity and density in time-domain full waveform inversion: 84th Annual International Meeting, SEG, Expanded Abstracts, 922–927, http://dx.doi.org/10.1190/segam2014-0532.1.

Beylkin, G., 1985, Imaging of discontinuities in the inverse scattering problem by inversion of a causal generalized radon transform: Journal of Mathematical Physics, **26**, 99–108, http://dx.doi.org/10.1063/1.526755.

Bleistein, N., 1987, On the imaging of reflectors in the earth: Geophysics, **52**, 931–942, http://dx.doi.org/10.1190/1.1442363.

Bleistein, N., J. K. Cohen, and J. W. Stockwell, 2001, Mathematics of multidimensional seismic imaging, migration, and inversion: Springer-Verlag, Inc.

Forgues, E., and G. Lambaré, 1997, Parameterization study for acoustic and elastic ray born inversion: Journal of Seismic Exploration, **6**, 253–277.

Gardner, G. H. F., L. W. Gardner, and A. R. Gregory, 1974, Formation velocity and density – The diagnostic basics for stratigraphic traps: Geophysics, **39**, 770–780, http://dx.doi.org/10.1190/1.1440465.

Giboli, M., R. Baina, L. Nicoletis, and B. Duquet, 2012, Reverse time migration surface offset gathers part 1: A new method to produce classical common image gathers: 82nd Annual International Meeting, SEG, Expanded Abstracts, http://dx.doi.org/10.1190/segam2012-1007.1.

Guillaume, P., G. Lambaré, S. Sioni, X. Zhang, A. Prescott, D. Carotti, P. Dépré, S. Frehers, and H. Vosberg, 2012, Building detailed structurally conformable velocity models with high definition tomography: 74th Annual International Conference and Exhibition, EAGE, Extended Abstracts, W002.

Guitton, A., 2004, Amplitude and kinematic corrections of migrated images for non-unitary imaging operators: Geophysics, **69**, 1017–1024, http://dx.doi.org/10.1190/1.1778244.

Guitton, A., 2014, On the velocity-density ambiguity in acoustic full-waveform inversion: 76th Annual International Conference and Exhibition, EAGE, Extended Abstracts, We-E106-03.

Jeong, W., and D. J. Min, 2012, Application of acoustic full waveform inversion for density estimation: 82nd Annual International Meeting, SEG, Expanded Abstracts, http://dx.doi.org/10.1190/segam2012-0196.1..

Kumar, R., B. Bai, and Y. Huang, 2014, Using reflection data for full waveform inversion – A case study from Santos basin: 76th Annual International Conference and Exhibition, EAGE, Expanded Abstracts, Th-E106-15.

Martin, G. S., R. Wiley, and K. J. Marfurt, 2006, Marmousi 2: An elastic upgrade for Marmousi: The Leading Edge, **25**, 156–166, http://dx.doi.org/10.1190/1.2172306.

Plessix, R. E., P. Milcik, H. Rynja, A. Stopin, K. Matson, and S. Abri, 2013, Multiparameter full-waveform inversion: Marine and land examples: The Leading Edge, **32**, 1030–1038, http://dx.doi.org/10.1190/tle32091030.1.

Przebindowska, A., A. Kurzmann, D. Kohn, and T. Bohlen, 2012, The role of density in acoustic full waveform inversion of marine reflection seismics: 74th Annual International Conference and Exhibition, EAGE, Extended Abstracts, W027.

Qin, B., T. Allemand, and G. Lambaré, 2015, Full waveform inversion using preserved amplitude reverse time migration: 85th Annual International Meeting, SEG, Expanded Abstracts, 1252–1257, http://dx.doi.org/10.1190/segam2015-5865645.1.

Tarantola, A., 1984, Inversion of seismic reflection data in the acoustic approximation: Geophysics, **49**, 1259–1266, http://dx.doi.org/10.1190/1.1441754.

Virieux, J., and S. Operto, 2009, An overview of full-waveform inversion in exploration geophysics: Geophysics, **74**, no. 6, WCC1–WCC26, http://dx.doi.org/10.1190/1.3238367.

Zhang, Y., A. Ratcliffe, G. Roberts, and L. Duan, 2014, Amplitude-preserving reverse time migration: From reflectivity to velocity and impedance inversion: Geophysics, **79**, no. 6, S271–S283, http://dx.doi.org/10.1190/geo2013-0460.1.